Convection in a layer heated from below with a nearly insulating boundary

R. M. Clever and F. H. Busse
Institute of Geophysics and Planetary Physics, University of California at Los Angeles, Los Angeles, California 90024
and Institute of Physics, University of Bayreuth, D-95440 Bayreuth, Germany
(Received 29 September 1997)

The problem of two- and three-dimensional finite amplitude thermal convection in a fluid layer heated from below is analyzed in the case when one boundary has a much higher and the other boundary has a much lower thermal conductivity than the fluid. Both stress-free and no-slip boundary conditions for the velocity field are considered. It is shown that two-dimensional convection rolls are stable for Rayleigh numbers not too far above the critical value R_c for the onset of convection. But at a Rayleigh number R_{II} less than twice the critical value they become unstable and are replaced by hexaroll convection. (Here ''hexarolls'' denotes a new planform intermediate to hexagons and rolls.) At an even higher value of R time dependent convection is found. [S1063-651X(98)04904-6]

PACS number(s): 47.20.Bp, 47.20.Ky, 47.27.Te, 47.54.+r

I. INTRODUCTION

Traditionally the problem of Rayleigh-Bénard convection in a fluid layer heated from below has been considered for boundaries with high thermal conductivity such that the boundary temperatures could be regarded as fixed. It has been known for some time, however, that the thermal conductivity of the boundary may have a strong influence on the type of convection flow that is realized in the fluid layer. When both boundaries are much less conducting than the fluid, the wavelength of convection flow becomes very large in comparison with the height of the layer [1] and square pattern convection will be realized instead of two-dimensional convection rolls [2,3]. When one boundary has a very high thermal conductivity and the other a very low one then a new instability of convection rolls enters and leads to the replacements of rolls by a three-dimensional pattern of convection, which has been called hexaroll convection in [4]. This result was found in the case of a highly conducting no-slip lower boundary and a stress-free nearly insulating upper boundary [4]. The goal of the present paper is to generalize these results and to explore the stability properties of the hexaroll patterns.

The paper starts with a brief outline in Sec. II of the mathematical problem and the numerical scheme used for the approximation of solutions. Three different combinations of boundary conditions are then explored in Secs. III–V, the last of which extends the work of Ref. [4] into the domain of time dependent convection. The paper finishes with an outlook on future work and possible laboratory experiments.

II. MATHEMATICAL FORMULATION OF THE PROBLEM

We consider horizontal fluid layers of thickness d heated from below with three different types of boundary conditions. Case A corresponds to a lower rigid boundary with a prescribed temperature T_2 and an upper stress-free boundary which is nearly thermally insulating. For the static solution of pure conduction the constant temperature T_1 will be realized at this latter boundary. In case B the thermal properties of the two boundaries are reversed such that the temperature T_1 at the upper stress-free boundary is now prescribed. In the third case C both boundaries are assumed to be rigid. The results of the analysis in the latter case will be the same whether the lower boundary is nearly insulating and the upper is highly conducting or vice versa because we are assuming the Boussinesq approximation. For simplicity we shall use a lower nearly insulating boundary in case C. It is possible, of course, to consider the problem with two stress-free boundaries. But since the realization of such a case is experimentally difficult—though not impossible (see Goldstein and Graham, [5])—and because it does not offer special theoretical advantages, we shall not pursue it here. The simple analytical solutions that are possible when symmetric highly conducting or nearly insulating boundaries are used disappear, of course, when asymmetric combinations of boundary conditions are assumed.

Using d as length scale, d^2/κ as time scale, where κ is the thermal diffusivity, and T_2-T_1 as scale of the temperature, we write the equations of motion for the velocity vector $\boldsymbol{u}$ and the heat equation for the deviation Θ of the temperature from its static distribution in dimensionless form,

$$\left(\frac{\partial}{\partial t}\boldsymbol{u}+\boldsymbol{u}\cdot\nabla\boldsymbol{u}\right)P^{-1}=-\nabla\pi+R\Theta\boldsymbol{k}+\nabla^2\boldsymbol{u}, \tag{1a}$$

$$\nabla\cdot\boldsymbol{u}=0, \tag{1b}$$

$$\left(\frac{\partial}{\partial t}+\boldsymbol{u}\cdot\nabla\right)\Theta=\boldsymbol{u}\cdot\boldsymbol{k}+\nabla^2\Theta, \tag{1c}$$

where $\boldsymbol{k}$ is the vertical unit vector and where the Prandtl number P and the Rayleigh number R satisfy the definitions

$$P=\nu/\kappa, \quad R=\gamma g(T_2-T_1)d^3/\kappa\nu. \tag{2}$$

g denotes the acceleration of gravity, γ is the thermal expansivity, and ν is the kinematic viscosity. Using a Cartesian system of coordinates with the z coordinate in the direction of $\boldsymbol{k}$, we write the boundary conditions for the three cases, A, B, and C, in the following form:

case A:

$$\boldsymbol{u}=0, \quad \Theta=0 \quad \text{at} \quad z=0, \tag{3a}$$

$$\frac{\partial}{\partial z}\boldsymbol{k}\times\boldsymbol{u}=0, \quad \boldsymbol{u}\cdot\boldsymbol{k}=\overline{\Theta}=\frac{\partial}{\partial z}(\Theta-\overline{\Theta})=0 \quad \text{at} \quad z=1, \tag{3b}$$

case B:

$$\boldsymbol{u}=0, \quad \overline{\Theta}=\frac{\partial}{\partial z}(\Theta-\overline{\Theta})=0 \quad \text{at} \quad z=0, \tag{4a}$$

$$\frac{\partial}{\partial z}\boldsymbol{k}\times\boldsymbol{u}=0, \quad \boldsymbol{u}\cdot\boldsymbol{k}=\Theta=0 \quad \text{at} \quad z=1, \tag{4b}$$

case C:

$$\boldsymbol{u}=0, \quad \overline{\Theta}=\frac{\partial}{\partial z}(\Theta-\overline{\Theta})=0 \quad \text{at} \quad z=0, \tag{5a}$$

$$\boldsymbol{u}=0, \quad \Theta=0 \quad \text{at} \quad z=1, \tag{5b}$$

where $\overline{\Theta}$ indicates the horizontal average of Θ. We have made use of the property that the Rayleigh number is based on the average temperature at the nonconducting boundary which requires the vanishing of $\overline{\Theta}$ at this boundary. The continuation of the temperature field into the nearly insulating boundary which is assumed to extend over a vertical distance of several heights of the fluid layer then leads to the boundary condition for the fluctuating component of the temperature field as has been discussed in [4].

To solve the problems posed by Eq. (1) together with the three types of boundary conditions (3), (4), and (5) we first eliminate the equation of continuity by introducing the general representation for the solenoidal velocity field

$$\boldsymbol{u}=\nabla\times(\nabla\times\boldsymbol{k}\phi)+\nabla\times\boldsymbol{k}\psi+\boldsymbol{U}(z), \tag{6}$$

where the mean velocity field $\boldsymbol{U}$ usually vanishes. We shall return to the possibility of a mean flow in Sec VII. By taking the z component of the curl and of the $(\text{curl})^2$ of Eq. (1a) we obtain two scalar equations for ϕ and ψ,

$$\nabla^4\Delta_2\phi-R\Delta_2\Theta=P^{-1}\left(\boldsymbol{k}\cdot\nabla\times(\nabla\times\boldsymbol{u}\cdot\nabla\boldsymbol{u})+\frac{\partial}{\partial t}\nabla^2\Delta_2\phi\right), \tag{7a}$$

$$\nabla^2\Delta_2\psi=P^{-1}\left(-\boldsymbol{k}\cdot\nabla\times(\boldsymbol{u}\cdot\nabla\boldsymbol{u})+\frac{\partial}{\partial t}\Delta_2\psi\right). \tag{7b}$$

To obtain steady solutions for Eqs. (7), (1c) we employ the Galerkin method and expand the dependent variables in complete systems of functions that satisfy all boundary conditions,

$$\phi=\sum_{l,m,n}^{\infty} a_{lmn}\exp\{il\alpha_x x+im\alpha_y y\}g_n(z), \tag{8a}$$

$$\psi=\sum_{l,m,n}^{\infty} c_{lmn}\exp\{il\alpha_x x+im\alpha_y y\}h_n(z), \tag{8b}$$

$$\Theta=\sum_{l,m,n}^{\infty} b_{lmn}\exp\{il\alpha_x x+im\alpha_y y\}f_n(z)+\sum_{n=1}^{\infty} b_{00n}\sin n\pi z, \tag{8c}$$

where the summation over l,m runs through all integer values except for the combination $m=l=0$ and the summation over n runs through all positive integers. The functions f_n, g_n, h_n assume the form

$$\left.\begin{aligned} f_n&=h_n=\sin(n-\tfrac{1}{2})\pi z \\ g_n&=\frac{\sinh\beta_n(1-z)}{\sinh\beta_n}-\frac{\sin\beta_n(1-z)}{\sin\beta_n}\end{aligned}\right\} \quad \text{for} \quad n=1,\ldots,\infty \quad \text{in case A,} \tag{9a}$$

$$\left.\begin{aligned} f_n&=\sin(n-\tfrac{1}{2})\pi(z-1), \quad h_n=\sin(n-\tfrac{1}{2})\pi z \\ g_n&=\frac{\sinh\beta_n(1-z)}{\sinh\beta_n}-\frac{\sin\beta_n(1-z)}{\sin\beta_n}\end{aligned}\right\} \quad \text{for} \quad n=1,\ldots,\infty \quad \text{in case B,} \tag{9b}$$

$$\left.\begin{aligned} f_n&=\sin(n-\tfrac{1}{2})\pi(z-1), \quad h_n=\sin n\pi z \quad \text{for} \quad n=1,\ldots, \\ g_n&=\frac{\sinh\gamma_n(z-\frac{1}{2})}{\sinh\frac{1}{2}\gamma_n}-\frac{\sin\gamma_n(z-\frac{1}{2})}{\sin\frac{1}{2}\gamma_n} \quad \text{for even} \quad n \\ &=\frac{\cosh\gamma_n(z-\frac{1}{2})}{\cosh\frac{1}{2}\gamma_n}-\frac{\cos\gamma_n(z-\frac{1}{2})}{\cos\frac{1}{2}\gamma_n} \quad \text{for odd} \quad n\end{aligned}\right\} \quad \text{in case C.} \tag{9c}$$

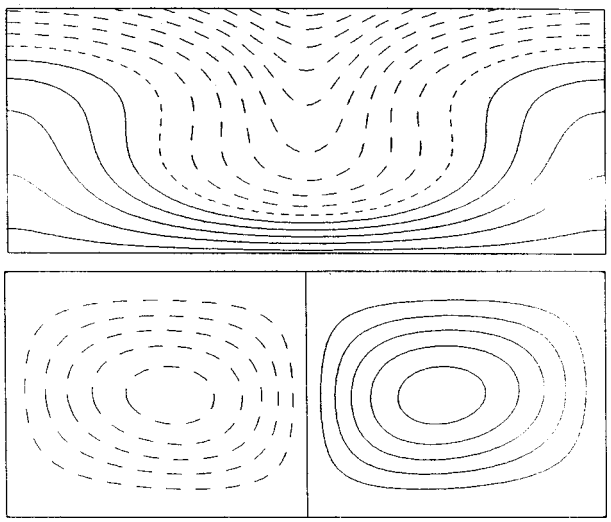

FIG. 1. Isotherms (upper plot) and streamlines (lower plot) of convection rolls in a layer with upper rigid insulating and lower rigid isothermal boundary for $R=3000$, $\alpha=2.55$, $P=0.71$.

The numbers β_n, γ_n are obtained as ordered roots of the equations

$$\coth \beta_n - \cot \beta_n = 0 \quad \text{for} \quad n=1,\ldots,\infty,$$

$$\coth \frac{1}{2}\gamma_n - \cot \frac{1}{2}\gamma_n = 0 \quad \text{for even} \quad n,$$

$$\tanh \frac{1}{2}\gamma_n + \tan \frac{1}{2}\gamma_n = 0 \quad \text{for odd} \quad n.$$

After projection of Eqs. (7) and (1c) onto the systems of expansion functions (8) a system of nonlinear algebraic equations for the unknown coefficients a_{lmn}, b_{lmn}, and c_{lmn} is obtained which can be solved by the Newton-Raphson iteration method after a truncation scheme has been introduced. Following earlier work of this kind we shall neglect all coefficients and corresponding equations with subscripts satisfying

$$l+m+n > N_T,$$

where the truncation parameter N_T must be chosen sufficiently large such that properties of physical interest do not change significantly when N_T is replaced by N_T-2.

The stability of steady solutions of the form (8) can be studied through the imposition of infinitesimal disturbances

$$\tilde{\phi} = \exp\{ibx+idy+\sigma t\} \sum_{l,m,n} \tilde{a}_{lmn} \exp\{il\alpha_x x + im\alpha_y y\} g_n(z), \tag{10a}$$

$$\tilde{\psi} = \exp\{ibx+idy+\sigma t\} \sum_{l,m,n} \tilde{c}_{lmn} \exp\{il\alpha_x x + im\alpha_y y\} h_n(z), \tag{10b}$$

$$\tilde{\Theta} = \exp\{ibx+idy+\sigma t\} \sum_{l,m,n} \tilde{b}_{lmn} \exp\{il\alpha_x x + im\alpha_y y\} f_n(z), \tag{10c}$$

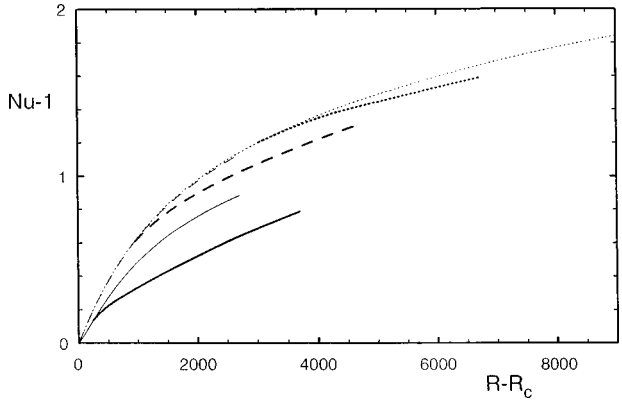

FIG. 2. Nusselt number Nu as a function of the Rayleigh number R for convection in case C with $P=0.1$ (solid lines), $P=0.71$ (dashed curves), and $P=2.5$ (dotted curves). The thin lines apply for rolls ($\alpha_y=2.4$), thick lines apply to hexarolls ($\alpha_x=\alpha_y=1.2$).

where in contrast to the summation in expressions (8) the case $l=m=0$ must be included in the summation. Only in the exceptional case $b=d=0$ must we drop the coefficients with subscripts $l=m=0$ and add the sum

$$\sum_n \tilde{b}_{00n} \sin n\pi z$$

in expression (10c). According to Floquet theory, expressions (10) represent the most general ansatz for infinitesimal disturbances. After projection of the linearized equations for the disturbances onto the system of expansion functions a system of linear homogeneous algebraic equations for the unknown coefficients $\tilde{a}_{lmn}, \tilde{b}_{lmn}, \tilde{c}_{lmn}$ is obtained with the growth rate σ as eigenvalue. For a given steady solution of the form (8) with the parameters R, P, α_x, α_y the eigenvalue σ can be determined as a function of b and d. Whenever there exists an eigenvalue σ with positive real part σ_r the steady solution is unstable. Otherwise we shall regard it as stable.

III. STEADY CONVECTION ROLLS

The boundary condition for the temperature at the nearly insulating boundary is less constraining than at a well conducting boundary corresponding to $\Theta=0$. It thus must be expected that the critical value for the onset of convection is lower when a well conducting boundary is replaced by a nearly insulating one. The critical values obtained in the three cases are as follows:

case A:

$$R_c = 669.00, \quad \alpha_c = 2.09, \tag{11a}$$

case B:

$$R_c = 816.75, \quad \alpha_c = 2.215, \tag{11b}$$

case C:

$$R_c = 1295.78, \quad \alpha_c = 2.552 \tag{11c}$$

in agreement with the values of [1]. In order to describe two-dimensional convection rolls we use representation (8) with

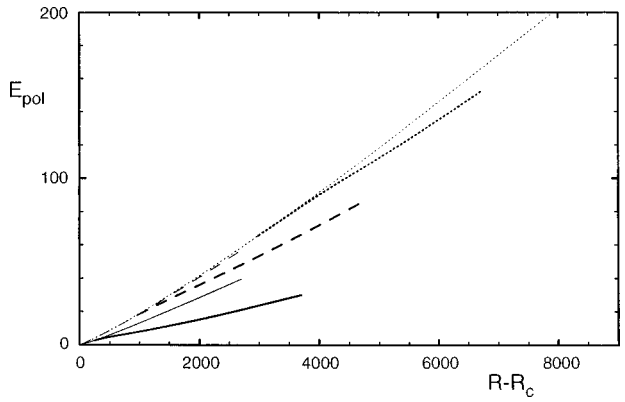

FIG. 3. Same as Fig. 2, but for the kinetic energy $E_{\rm pol}$ instead of Nu.

$$a_{lmn}=b_{lmn}=c_{lmn}=0 \quad \text{for} \quad l\neq 0 \tag{12a}$$

and

$$a_{0-mn}=a_{0mn}, \quad b_{0-mn}=b_{0mn}, \quad c_{0mn}=0 \quad \text{for all} \quad m,n, \tag{12b}$$

where the latter condition anticipates the existence of a vertical plane of symmetry for the rolls. While the convection at onset is not very different from that found in layers with fixed temperatures at the boundaries, the distribution of isotherms changes rather strongly as the amplitude of convection increases. As indicated in Fig. 1 the isotherms are pulled into the interior of the layer from the nearly insulating boundary such that the horizontal gradient of the temperature tends to exceed the vertical one.

In Fig. 2 the convective heat transport given by the Nusselt number Nu has been plotted as a function of the Rayleigh number. The curves for case C show a similar dependence as the curve obtained for case A in [4]. The corresponding curves for the kinetic energy are shown in Fig. 3. Since the toroidal component of motion vanishes for

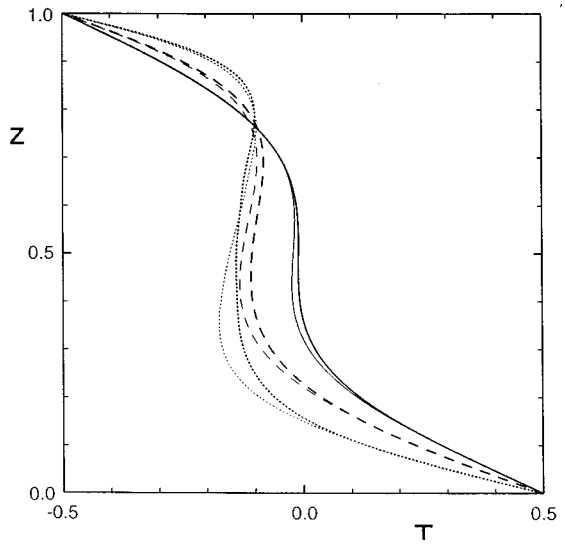

FIG. 4. The horizontally averaged temperature as a profile of height z in cases B with $R=4000$ (dashed lines) and $R=15\,000$ (dotted lines) and in case C with $R=4000$ (solid lines) for $P=0.71$ (thick lines) and $P=7.0$ (thin lines).

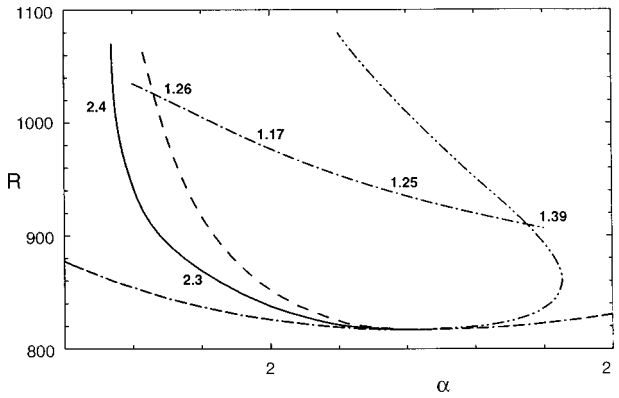

FIG. 5. Stability boundaries of two-dimensional rolls in case B for $P=0.71$. The domain of stable rolls is bounded by the onset of the Eckhaus instability (dashed line), by the onset of the subharmonic varicose instability (dash-dotted line), and by the onset of the skewed varicose instability (dash-double-dotted line). Also shown are the cross-roll instability boundary (solid line) and the neutral curve for the onset of convection (double-dash-dotted line). The numbers denote the values of b at the onset of instability.

rolls, $\psi\equiv 0$, the kinetic energy is given by

$$E_{\rm pol}=\frac{1}{2}\langle|\nabla\times(\nabla\times\boldsymbol{k}\phi)|^2\rangle, \tag{13}$$

where the angular brackets indicate the average over the fluid layer. Profiles of the mean temperature are shown in Fig. 4 for cases B and C. For profiles in case A see Fig. 5 of [4]. Please notice that the z interval $-0.5\leqslant z\leqslant 0.5$ has been used incorrectly in the latter figure instead of $0\leqslant z\leqslant 1$. The profiles in case C are nearly antisymmetric about the center of the layer while in cases A and B the average temperature of the layer is shifted towards the mean temperature of the upper stress-free boundary. This property indicates that the asymmetry of the velocity boundary conditions has a much stronger influence on the mean temperature profile than the asymmetry of the temperature boundary conditions.

IV. INSTABILITIES OF CONVECTION ROLLS

The onset of instabilities of various types is shown as a function of R and α in Figs. 5 and 6 for cases B and C with $P=0.71$. All lines in this diagram indicate locations at which the maximum real part σ_r of the growth rate σ goes through

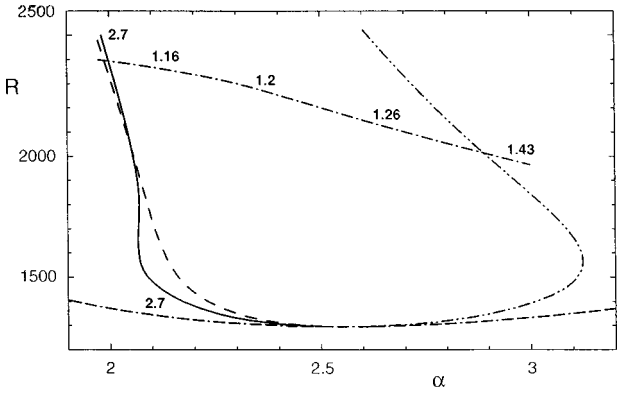

FIG. 6. Same as Fig. 5, but in case C.

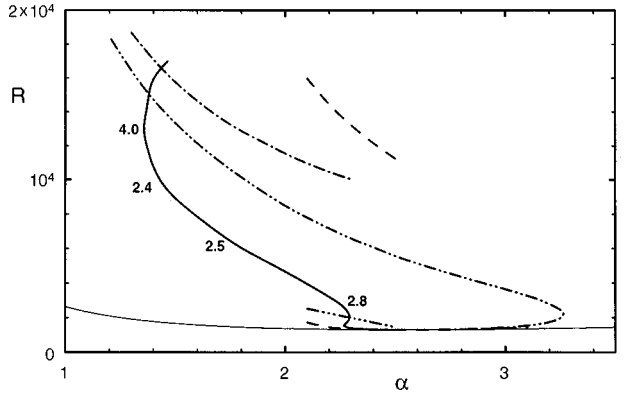

FIG. 7. Same as Fig. 5, but in case C for $P=7$.

zero. The qualitative features of these diagrams resemble those found in the standard Rayleigh-Bénard problem [6] except for the new subharmonic varicose instability boundary which appears to be typical for layers with strongly asymmetric temperature boundary conditions. As in the case A treated in [4], this instability leads to the onset of hexaroll convection as we shall discuss in the next section. The maximum growth rate of this instability is always reached for the value $d=\alpha_y/2$ and for finite values of b which have been indicated in Figs. 5 and 6. In the case of $P=7$ for which only the stability diagram for case C has been computed, the subharmonic varicose instability is preceded by the knot instability as shown in Fig. 7. We thus conclude that the additional asymmetry of the velocity boundary condition in case A contributes just a little bit to promote the onset of the subharmonic varicose instability as shown in Fig. 6 of [4].

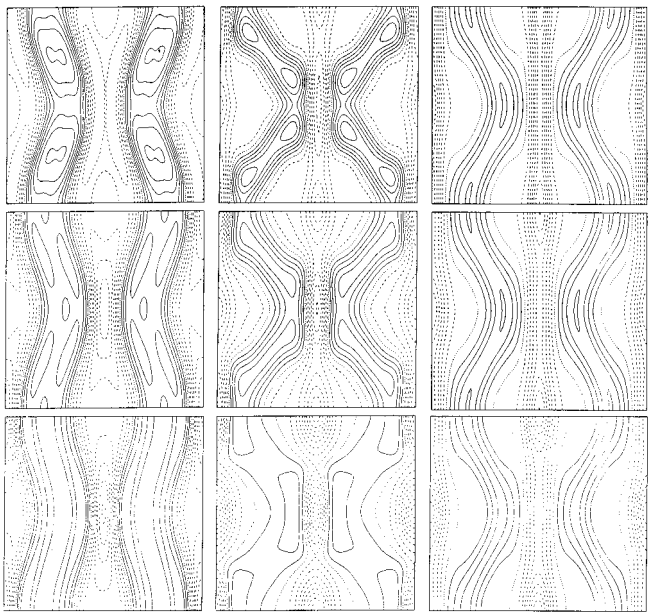

FIG. 8. Lines of constant vertical velocity in the planes $z=0.9$ (top row), $z=0.5$ (middle row), and $z=0.1$ (bottom row) of hexaroll solutions in case C for $P=0.1$, $R=1700$ (left column), $P=0.71$, $R=5000$ (middle column), and $P=2.5$, $R=6000$ (right column). The wave numbers are $\alpha_x=\alpha_y=1.2$ in all cases except in the case $P=2.5$ where $\alpha_y=1.1$ (y direction is left to right).

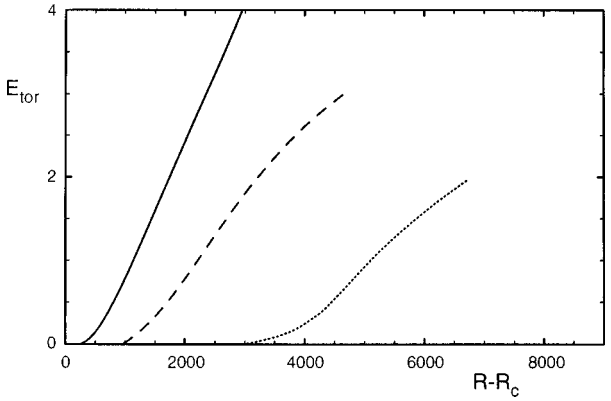

FIG. 9. The kinetic energy of the toroidal component of the velocity for hexaroll convection as a function of R in case C with $P=0.1$ (solid line), $P=0.71$ (dashed line), and $P=2.5$ (dotted curve). In all cases $\alpha_x=\alpha_y=1.2$ has been used.

V. STEADY HEXAROLL CONVECTION

The nature of the subharmonic varicose instability may suggest a transition from rolls to hexagonal convection cells since the strongest growth is found for values of b close to $\sqrt{3}\alpha_y/2$. But an intermediate pattern between rolls and hexagons evolves as asymptotic steady state from the growing disturbances. This solution has been called the hexaroll solution and is described by representation (8) with the following symmetry properties:

$$a_{lmn}=b_{lmn}=c_{lmn}=0 \quad \text{for} \quad l+m=\text{odd}, \tag{14a}$$

$$a_{-lmn}=a_{lmn}, b_{-lmn}=b_{lmn}, c_{-lmn}=-c_{lmn}, \tag{14b}$$

$$a_{l-mn}=a_{lmn}, b_{l-mn}=b_{lmn}, c_{l-mn}=-c_{lmn}. \tag{14c}$$

In representation (8) α_y now denotes half the value of α_y of the roll solution from which the hexarolls bifurcate. In Fig. 8 hexaroll convection is shown for various Prandtl numbers in case C. The heat transport of hexarolls is less than that of the two-dimensional rolls from which they evolve as is evident from Fig. 2. The same property holds for the energy of the

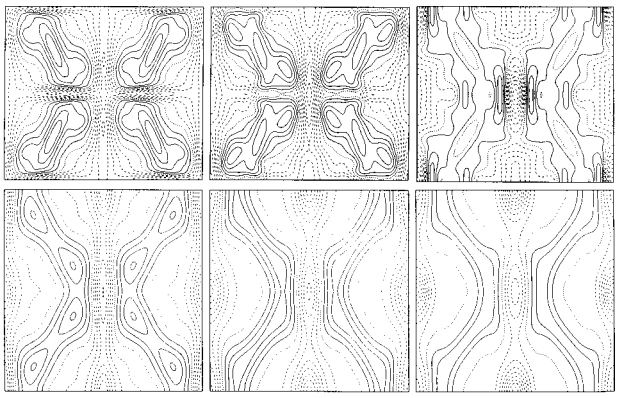

FIG. 10. Lines of constant vertical velocity in the horizontal planes $z=0.9,0.5,0.1$ (left to right) of the hexaroll solution in case A with the parameters $P=0.1$, $R=2500$, $\alpha_x=1.25$, $\alpha_y=1.1$ (upper row) and $P=2.5$, $R=4000$, $\alpha_x=\alpha_y=1.0$ (y direction is left to right).

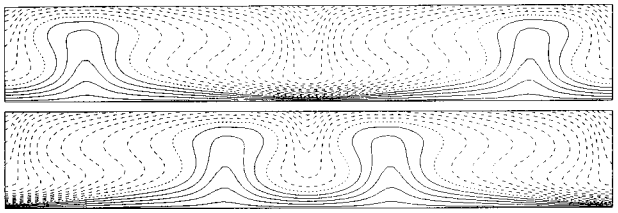

FIG. 11. Isotherms in the vertical planes $x=0$ (upper plot) and $x=\pi/\alpha_x$ (lower plot) for the hexaroll solution in case A with $P=2.5$, $R=4000$, $\alpha_x=\alpha_y=1.0$.

poloidal component of motion as can be seen in Fig. 3. Part of the kinetic energy resides now in the energy of the toroidal component of motion

$$E_{\rm tor}\equiv\frac{1}{2}\langle|\nabla\times\boldsymbol{k}\psi|^2\rangle \tag{15}$$

shown in Fig. 9. But the latter energy always remains a small fraction of $E_{\rm pol}$. The hexaroll solution in case A is shown in Fig. 10 for two different Prandtl numbers. A split of the area of rising motion into four sections can be noticed in the case of $P=0.1$, at least in the upper part of the layer. A similar tendency, but much weaker, can also be observed for $P=0.1$ in case C when the Rayleigh number is increased. In general it appears that the morphology of the convection motion depends more strongly on the Prandtl and on the Rayleigh number than on the velocity condition at the upper boundary. Because of the large area occupied by the descending plume even more isotherms are pulled in from the nearly insulating upper boundary by hexaroll convection than by rolls as can be seen from Fig. 11. But in case A as well as in case C the heat transport of the hexaroll solution is less than that of the corresponding roll solution as is demonstrated in Fig. 12. Three typical values of the Prandtl number P have been chosen to indicate the variation of the heat transport with P. As in other problems of convection with at least one rigid boundary, the heat transport by convection rolls varies very little for $P\geqslant 1$ and decreases with decreasing Prandtl number for $P<1$. A similar dependence can be

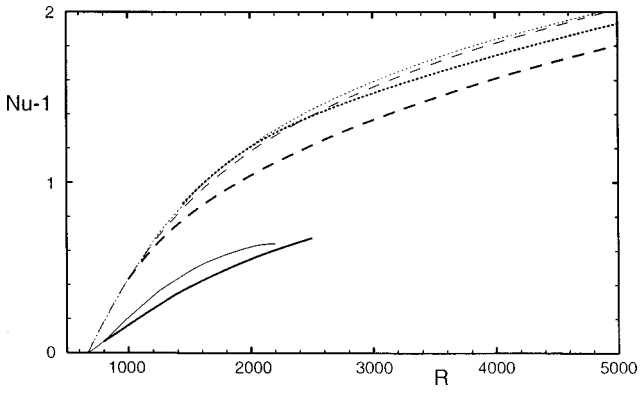

FIG. 12. Nusselt number Nu as a function of the Rayleigh number for rolls (thin lines) and steady hexaroll convection (thick lines) in case A for $P=0.1$ ($\alpha_x=1.25$, $\alpha_y=1.1$; solid lines), $P=0.71$ ($\alpha_x=1.2$, $\alpha_y=1.1$; dashed lines), and $P=2.5$ ($\alpha_x=1.0$, $\alpha_y=1.0$; dotted lines). The basic roll wave number is given by $2\alpha_y$.

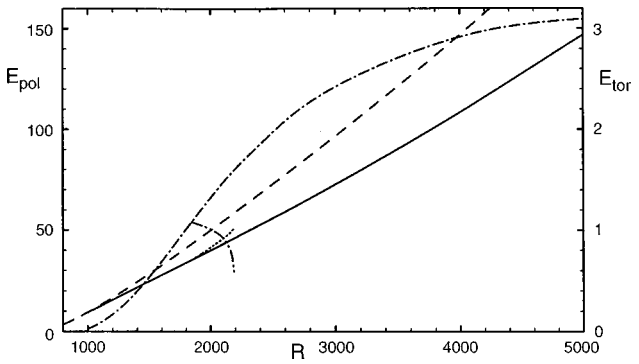

FIG. 13. Kinetic energies of the poloidal component of motion $E_{\rm pol}$ (solid line for rolls, dashed line for hexarolls, and dotted line for asymmetric drifting hexarolls), and of the toroidal component of motion $E_{\rm tor}$ (dash-dotted line for hexarolls, dash-double-dotted line for asymmetric drifting hexarolls) in case A with $P=0.71$, $\alpha_x=1.2$, $\alpha_y=1.1$.

found for the poloidal kinetic energy which has been plotted in Fig. 13 for $P=0.71$ only. The main effect of the Prandtl number on the properties of convection is due to the dependence on P of the transition from two- to three-dimensional flows as is evident from Fig. 12 and from the comparisons of Figs. 6 and 7.

VI. INSTABILITIES OF STEADY HEXAROLLS

The stability of the steady hexaroll solutions can be studied with the same general method as in the case of rolls. But the use of the full representation (10) for the disturbances leads to huge matrices for the determination of the growth rates σ. Since the basic rectangular periodicity interval $0\leqslant x<2\pi/\alpha_x$, $0\leqslant y<2\pi/\alpha_y$ already covers the horizontal area of two hexaroll cells, it is likely that subharmonic instabilities will not play an important role and that the major mechanisms of instability will correspond to the case $b=d=0$. Using this assumption we gain a major numerical advantage in that the disturbances separate into eight classes because of the symmetries (14) of the steady hexaroll solutions. Denoting the symmetries (14a), (14b), (14c) by e, C, C, respectively, we denote the opposite symmetries

$$a_{lmn}=b_{lmn}=c_{lmn}=0 \quad \text{for} \quad l+m=\text{even} \quad (o), \tag{16a}$$

TABLE I. Instabilities of steady hexaroll convection.

Case	P	α_x	α_y	$R_{\rm III}$	ω	Symmetry
A	0.1	1.25	1.1	944	1.54	oCS
	0.71	1.2	1.1	1846	0	eCS
	0.71	1.4	1.1	1807	0	oSC
	2.5	1.0	1.0	2494	0	eCS
				also unstable for		
				$1729<R<1969$		eSC
C	0.1	1.2	1.2	2221	1.90	eCC
	0.71	1.2	1.2	4961	0	eSC
	2.5	1.2	1.1	≈ 8400	0	eCC

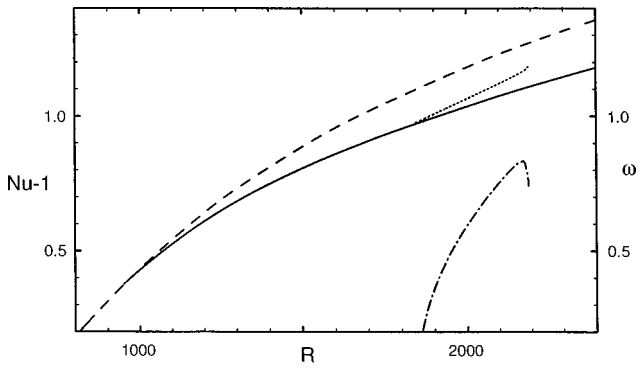

FIG. 14. Nusselt number for the same case as in Fig. 13. Also shown is the frequency of the drifting asymmetric hexarolls.

$$a_{-lmn}=-a_{lmn},b_{-lmn}=-b_{lmn},c_{-lmn}=c_{lmn} \quad (S), \tag{16b}$$

$$a_{l-mn}=-a_{l-mn},b_{l-mn}=-b_{lmn},c_{l-mn}=c_{lmn} \quad (S), \tag{16c}$$

by o,S,S as indicated. The eight symmetry classes of disturbances are now given by

$$eCC,eCS,eSC,eSS,oCC,oCS,oSC,oSS \tag{17}$$

depending on whether they share the respective symmetry with the steady hexarolls or not. Neither a complete exploration of the region of existence of steady hexaroll solutions in the α_x-α_y-R-P parameter space nor an investigation of the region of stability within the region of existence has been undertaken. Instead the hexaroll solutions have been explored with the wave numbers α_x and α_y fixed close to their critical values in cases A and C. The main results for the onset of instabilities of these solutions are listed in Table I.

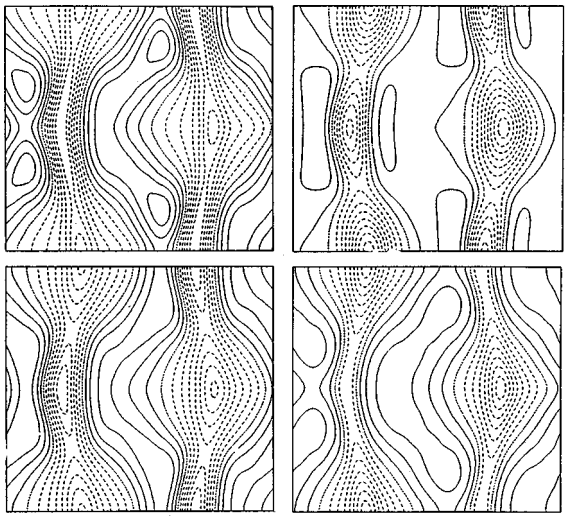

FIG. 15. Lines of constant vertical velocity in the planes $z=0.9$ (upper left), $z=0.5$ (lower left), and $z=0.1$ (upper right) and isotherms in the plane $z=0.5$ (lower right) for drifting asymmetric hexarolls in case A with $R=2000$, $P=0.71$, $\alpha_x=1.2$, $\alpha_y=1.1$.

TABLE II. Instabilities of drifting asymmetric hexarolls in case A with $P=0.71$, $\alpha_x=1.2$, $\alpha_y=1.1$.

R_{IV}	ω	Symmetry of disturbances
1989	0	$eSC+eSS$
2140	0	$oSC+oSS$

VII. TIME DEPENDENT HEXAROLL CONVECTION

The evolution of the instabilities listed in Table I has been followed through integration in time only in case A with $P=0.71$. For this purpose representation (8) is assumed with time dependent coefficients $a_{lmn}(t),b_{lmn}(t),c_{lmn}(t)$ and a system of ordinary differential equations in time is obtained in place of the system of nonlinear algebraic equations in the case of the steady hexaroll solutions. Although the onset of instability of the steady hexarolls at $R=1733$ occurs in the form of monotonously growing disturbances it evolves into an oscillatory form of convection at finite amplitude. The angular frequency ω is shown in Fig. 14 together with the Nusselt number in dependence on R. As must be expected on the basis of the stability analysis ω starts at zero; it ends at a finite value at a Rayleigh number of about 2191 where numerically convergent solutions ceased to exist. The oscillatory hexaroll solution actually corresponds to hexarolls drifting in the y direction as a shape preserving traveling wave. By replacing y by $y-ct$ with $c=\omega/\alpha_y$ the drifting hexarolls become steady with respect to the drifting frame of reference. Accordingly, the coefficients a_{lmn},b_{lmn},c_{lmn} can be obtained as solutions of algebraic equations just as in the case of the steady hexaroll solutions. Figure 15 shows an example of these solutions, called asymmetric drifting hexarolls, in the drifting frame of reference. There are always two drifting asymmetric hexaroll solutions differing only by the sign of the coefficients with the eCS symmetry in the solution. These two solutions correspond to opposite directions of the drift in the y direction and to opposite mean flows. Because the drifting hexarolls no longer possess a plane of symmetry, $y=\mathrm{const}$, as the steady hexarolls do which are symmetric with respect to plane $y=2n\pi/\alpha_y$ for all integer n, a mean flow in the y direction must be expected. The mean flow U_y obeys the equation

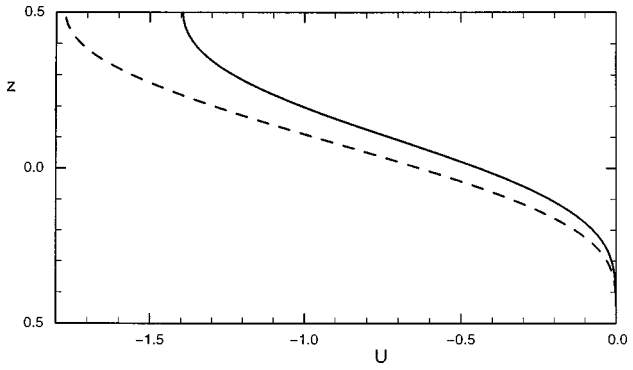

FIG. 16. Profiles of the mean flow in the y direction corresponding to drifting asymmetric hexarolls in case A with $P=0.71$, $\alpha_x=1.2$, $\alpha_y=1.1$ for the Rayleigh numbers $R=2000$ (solid line) and $R=2190$ (dashed line).

$$\left(\frac{\partial}{\partial t}-\frac{\partial^2}{\partial z^2}\right)U_y(z,t)=\overline{\Delta_2\phi(\partial_{yz}^2\phi-\partial_x\psi)}, \tag{18}$$

where the bar indicates the average over the x-y plane.

Because the asymmetric drifting hexarolls represented by modes of the symmetry classes eCC and eCS are steady in the appropriate reference frame, the stability analysis can be carried out in the same way as in the case of steady hexarolls. The difference is that the disturbances do not separate into eight classes when no changes in the horizontal periodicity are allowed as discussed in Sec. VI, but into four classes instead. These classes are

$$eCC+eCS, \quad eSC+eSS, \quad oCC+oCS, \quad oSC+oSS. \tag{19}$$

The stability analysis of asymmetric drifting hexarolls with respect to these classes of disturbances indicates an instability with respect to the first class of the four classes of disturbances as shown in Table II. Only at a much higher value of R do disturbances of the fourth class begin to grow. When the evolution of these growing disturbances is followed spatially and temporally chaotic convection flows are found. Of special interest is the mean flow connected with the traveling asymmetric hexaroll solutions. The profiles of the mean flow in the y direction are shown in Fig. 16 for two different Rayleigh numbers. Its direction changes with the direction of propagation of the asymmetric drifting hexarolls.

VIII. CONCLUDING REMARKS

A change in the boundary conditions of a fluid layer heated from below usually does not change the properties of the convection flow dramatically. There exist singular cases such as convection rolls in the presence of stress-free boundaries with fixed temperature which exhibit a finite increase of the convective heat transport in the limit of vanishing Prandtl number in contrast to all other forms of convection in this limit. But apart from this exception variations in the boundary conditions for the velocity field usually affect the properties of convection only in a quantitative way. Thermal boundary conditions can have a strong influence on the pattern of convection and on its dynamics as the analysis of this paper indicates. The appearance of three-dimensional hexaroll convection relatively close to the onset of convection and the transition to a drifting form of this convection are unusual at low Rayleigh numbers. The mean flow associated with the drifting pattern is of particular interest since processes that induce such features usually are found only at much higher Rayleigh numbers in convection layers. It thus is highly desirable that careful experiments are initiated for observations of the new features predicted by the theory of [4] and its extensions described in the present paper.

[1] E. M. Sparrow, R. J. Goldstein, and V. K. Jonsson, J. Fluid Mech. **18**, 513 (1964).
[2] F. H. Busse and N. Riahi, J. Fluid Mech. **96**, 243 (1980).
[3] M. R. E. Proctor, J. Fluid Mech. **113**, 469 (1981).
[4] R. M. Clever and F. H. Busse, Phys. Fluids **7**, 92 (1995).
[5] R. J. Goldstein and D. J. Graham, Phys. Fluids **12**, 1133 (1969).
[6] F. H. Busse and R. M. Clever, J. Fluid Mech. **91**, 319 (1979).